R.F. Dutra and F.S.F. Zinani and L.A.O. Rocha and C. Biserni

Effect of non-Newtonian fluid rheology on an arterial bypass graft: A numerical investigation guided by constructal design

In:

Computer Methods and Programs in Biomedicine, vol. 201, 2021, issn: 0169-2607.

The final published version is available online at:

https://doi.org/10.1016/j.cmpb.2021.105944

EFFECT OF NON-NEWTONIAN FLUID RHEOLOGY ON AN ARTERIAL BYPASS GRAFT: A NUMERICAL INVESTIGATION GUIDED BY CONSTRUCTAL DESIGN

R.F. Dutra[1], F.S.F. Zinani[1*], L.A.O. Rocha[1] and C. Biserni[2]

[1] *Mechanical Engineering Graduate Program, Universidade do Vale do Rio dos Sinos, 93022-750, São Leopoldo, Brazil.*

[2] *Department of Industrial Engineering (DIN), School of Engineering and Architecture, Alma Mater Studiorum - University of Bologna, Viale Risorgimento 2, 40136 Bologna, Italy*

[*]*corresponding author: cesare.biserni@unibo.it*

Abstract

In post-operative scenarios of arterial graft surgeries to bypass coronary artery stenosis, fluid dynamics plays a crucial role. Problems such as intimal hyperplasia have been related to fluid dynamics and wall shear stresses near the graft junction. This study focused on the question of the use of Newtonian and non-Newtonian models to represent blood in this type of problem in order to capture important flow features, as well as an analysis of the performance of geometry from the view of Constructive Theory. The objective of this study was to investigate the effects rheology on the steady-state flow and on the performance of a system consisting of an idealized version of a partially obstructed coronary artery and bypass graft. The Constructal Design Method was employed with two degrees of freedom: the ratio between bypass and artery diameters and the junction angle at the bypass inlet. The flow problem was solved numerically using the Finite Volume Method with blood modeled employing the Carreau equation for viscosity. The Computational Fluid Dynamics model associated with the Sparse Grid method generated eighteen response surfaces, each representing a severe stenosis degree of 75% for specific combinations of rheological parameters, dimensionless viscosity ratio, Carreau number and flow index at two distinct Reynolds numbers of 150 and 250. There was a considerable dependence of the pressure drop on rheological parameters. For the two Reynolds numbers studied, the Newtonian case presented the lowest value of the dimensionless pressure drop, suggesting that the choice of applying Newtonian blood may underestimate the value of pressure drop in the system by about 12.4% (Re =150) and 7.8% (Re = 250). Even so, results demonstrated that non-Newtonian rheological parameters did not influence either the shape of the response surfaces or the optimum bypass geometry, which consisted of a diameter ratio of 1 and junction angle of 30°. However, the viscosity ratio and the flow index had the greatest impact on pressure drop, recirculation zones and wall shear stress. Rheological parameters

also affected the recirculation zones downstream of stenosis, where intimal hyperplasia is more prevalent. Newtonian and most non-Newtonian results had similar wall shear stresses, except for the non-Newtonian case with high viscosity ratio. In the view of Constructal Design, the geometry of best performance was independent of the rheological model. However, rheology played an important role on pressure drop and flow dynamics, allowing the prediction of recirculation zones that were not captured by a Newtonian model.

Keywords: *Constructal Design, non-Newtonian blood, Carreau model, coronary artery bypass graft, dimensionless pressure drop.*

Nomenclature

D	artery diameter	[m]
D_0	stenosis diameter	[m]
D_1	graft diameter	[m]
D_{ij}	strain rate tensor	[s^{-1}]
$D_1/D,_{opt}$	optimum diameter ratio	[-]
L	artery length	[m]
M	surface response verification points	[-]
n	power law index	[-]
N	number of mesh elements	[-]
$\tilde{p}$	dimensionless pressure drop	[-]
$\tilde{p}_{min}$	minimum dimensionless pressure drop	[-]
Re	Reynolds number	[-]
S	stenosis degree	[-]
U_m	average velocity	[m s^{-1}]
u_i	velocity vector	[m s^{-1}]
$\tilde{u}_i$	dimensionless velocity field	[-]
V	artery volume	[m^3]
V_1	graft volume	[m^3]
$\tilde{X}$	dimensionless position	[-]
X	position vector	[m]

$\tilde{x}_i$	dimensionless position vector	[-]

Greek symbols

α	junction angle	[-]
$\alpha_{,opt}$	optimum junction angle	[-]
Δp	pressure drop	[Pa]
η	viscosity function	[Pa s]
η_c	characteristic viscosity	[Pa s]
η_0	zero shear rate viscosity	[Pa s]
η_∞	infinite shear rate viscosity	[Pa s]
$\tilde{\eta}$	dimensionless viscosity function	[-]
η^*	dimensionless viscosity ratio	[-]
λ	time constant	[-]
$\tilde{\lambda}$	Carreau number	[-]
μ	dynamic viscosity	[Pa s]
ρ	mass density	[kg m^{-3}]
$\dot{\gamma}$	shear rate	[s^{-1}]
τ^*	normalized shear stress	[-]
τ_{ij}	extra-stress tensor	[Pa]
$\tilde{\tau}_{ij}$	dimensionless extra vector tensor field	[-]

1 INTRODUCTION

Blood composition is defined as a suspension of red blood cells (RBC) and plasma with relatively low volume fractions of white blood cells and platelets (HORNER et al., 2018). According to Owens (2006), blood is a non-Newtonian fluid with shear-thinning, thixotropic and viscoelastic properties. Johnston et al. (2004) asserted that none of the viscosity models for blood fully expresses the effects of its complicated rheology. The blood properties are dependent on many factors, e.g., cell and oxygen concentrations, coagulation, and adhesion. Also, its viscosity varies with the percentage of the total blood volume occupied by RBC, which is known as hematocrit (PEREIRA et al., 2013).

Additionally, previous studies have shown that rheological parameters of blood vary from individual to individual and are directly influenced by other several factors, e.g., male or female, smoker or non-smoker, temperature, lipid loading, hypocaloric diet, cholesterol level and physical fitness index (CHO and KENSEY, 1991). Zydney et al. (1991) asserted that red cells deform at high shear rates, which decreases blood viscosity. At low shear rates, occurs the opposite, i.e., red cells aggregate and cause a substantial increase in viscosity. Marcinkowska-Gapinska et al. (2007) studied 100 blood samples of myocardial infarction survivors treated by different antithrombotic drugs. Results suggested that acenocoumarol treatment could influence red cell deformability and rouleaux formation, while aspirin treatment did not affect any blood properties.

Brun et al. (2011) concluded that physiology, not only pathology, is also closely related to hemorheology and might be an important modifier of blood viscosity factors. Guiraudou et al. (2013) demonstrated that the body mass index might increase plasma viscosity and red cell rigidity. Brun et al. (2016) confirmed that fat mass is an important RBC regulator for all cases and not only for obese subjects. Mehri et al. (2018) performed several experimental tests varying shear rate and different hematocrit percentages in a controlled microfluidic system. The effects of temperature, hematocrit, shear rate and viscosity on RBC aggregate sizes were studied and non-Newtonian parameters associated with power-law and Carreau models were obtained.

Given these circumstances, several authors have studied non-Newtonian blood behavior in the cardiovascular system, especially in stenotic arteries, bifurcations, and ramifications. Cho and Kensey (1991) applied a finite element method to study the effects of non-Newtonian viscosity on blood flow through a stenotic coronary arterial bifurcation. It was concluded that non-Newtonian effects must be considered at low Reynolds numbers, corresponding to a resting state. Gijsen et al. (1999) investigated the influence of non-Newtonian blood properties on velocity distributions in a 3D model of a carotid artery bifurcation. It was concluded that changes in velocity distribution caused by shear thinning properties were dependent on the alteration of the artery geometry, i.e., in this case, bifurcations and diameter variation.

Razavi et al. (2011) applied the index proposed by Johnston et al. (2004) in a numerical study of a carotid artery under symmetrical 30% – 60% stenosis with Newtonian and several non-Newtonian fluid models. It was concluded that the differences between models were relevant, especially at low inlet velocities. Bodnár et al. (2011) compared non-Newtonian models of flow in vessels obstructed by stenosis. The findings suggested that shear-thinning effects stood out in the recirculation zone downstream of stenosis and they were more predominant than blood viscoelastic effects.

Molla and Paul (2012) performed blood flow simulations in a 3D stenotic artery model with different blood fluid models. It was found that the recirculation zone in the region downstream of stenosis increased in the non-Newtonian models. Tian et al. (2013) simulated a 2D stenosed artery and determined that results for wall shear stress (WSS) and other shear parameters for a non-Newtonian fluid model were smaller than those obtained for the Newtonian model. Karimi et al. (2014) studied numerically the flow at a realistic aorta. It was suggested that several non-Newtonian fluid models for blood might be employed as alternatives, with the exception of the Cross model, which displayed significant discrepancies at specific points compared to the other models.

Fortuny et al. (2015) studied blood flow in a 3D popliteal vein model with a thrombotic mass. Results indicated that non-Newtonian effects were also relevant at higher blood flow rates, contrasting with previous studies. Weddell et al. (2015) studied a 3D idealized femoral artery tree and found differences in velocity, WSS and pressure parameters between Newtonian and Carreau-Yasuda models. Overall, it was demonstrated that Newtonian velocity profiles presented higher peaks than the non-Newtonian model. Also, pressure in the Newtonian model was lower than in the non-Newtonian one.

Apostolidis et al. (2016) showed significant differences between the numerical simulations of Newtonian and non-Newtonian models of a simplified left coronary artery, especially at low shear rate regimes. This phenomenon was attributed to the coupling that existed between the low and high shear rate areas in the flow which occurred mainly in constrictions and bifurcations. Doost et al. (2016) performed a numerical analysis in a human patient-specific left ventricle and suggested that non-Newtonian models had a significant influence on blood flow dynamics. It was also observed that the maximum WSS value for most non-Newtonian models was significantly higher than the Newtonian model. Iasiello et al. (2017) investigated non-Newtonian effects on the blood flow through an aorta-iliac bifurcation. It was demonstrated that the Newtonian model was more robust at higher velocities than lower ones. Saedi Ardahaie et al. (2018) examined a blood fluid flow containing nanoparticles in a porous artery affected by magnetic field. The effects of specific physical parameters of Brownian motion, thermophoresis and pressure gradient on temperature, velocity and nanoparticles concentration profiles were examined. It was denoted the importance of Brownian motion and thermophoresis in temperature profiles and nanoparticles concentration. Also, it was demonstrated that the increase of the magnetic field parameter led to a decrease in blood velocity.

However, fewer works have focused their analysis on the non-Newtonian effects on an arterial bypass grafts. Abraham et al. (2005) presented a numerical optimization study of non-Newtonian effects in an idealized 2D arterial bypass graft. It was concluded that the non-Newtonian effects did not present significant differences in optimal shapes. Chen et al. (2006) applied the Carreau-Yasuda model in a stenosed coronary bypass and concluded that significant differences must be considered between the non-Newtonian and Newtonian fluid flows in axial velocity profiles, secondary flow streamlines and WSS. Results from this study supported that these hemodynamic differences might have significant effects downstream of the host vessel stenosis where intimal hyperplasia occurs predominantly. Intimal hyperplasia is an abnormal propagation of smooth muscle cells that causes a reduction in the bypass diameter leading to a new occlusion (BASSIOUNY et al., 1992).

O´Callaghan et al. (2006) modeled blood using various constitutive equations and demonstrated that the choice of model had to be based according to the studied parameter, e.g., flow rate, steady or pulsatile flow and geometry. For the case studied (a 45º bypass), the various constitutive models identified areas of relative high/low WSS but their values were quantitatively different. Vimmr and Jonásová (2010) investigated an idealized 100% occluded 3D bypass graft model using the Carreau–Yasuda model and confirmed that the steady non-Newtonian flow presented significant differences not only in the values of WSS but particularly in the velocity profile and distribution.

On the other hand, Vimmr et al. (2013) performed a numerical study of single, double and triple aortocoronary bypass grafts. It was demonstrated that non-Newtonian effects on blood flow were not significantly distinct from the Newtonian model and it was concluded that the bypass diameter was the most important parameter for the flow and WSS distribution, regardless of the fluid model adopted. Kim et al. (2014) performed a numerical study in an idealized arteriovenous bypass graft and discovered that the hematocrit variation was an important parameter that influenced this specific graft's hemodynamic characteristics.

Although many works on literature indicated differences between the hemodynamic characteristics of the cardiovascular system, Newtonian or non-Newtonian influence on blood flow is still debatable, especially on arterial bypass graft designs. Furthermore, in most previous works that studied non-Newtonian behavior of blood, standard values for rheological parameters were adopted regardless of the model chosen and did not observe the variation that these parameters may suffer due to the several factors mentioned previously.

In this regard, this study aims to investigate the influence of each rheological parameter of a Carreau fluid model for blood through the Constructal Design of an idealized arterial

bypass graft subjected to steady blood flow. This is a companion study to a previous study (DUTRA et al., 2020) that demonstrated, through the Constructal Design method, the influence of geometric parameters on the same graft design. In Dutra et al. (2020), the junction angle and diameter ratio between the bypass graft and artery were the degrees of freedom used to seek out configurations with best performance. It was found that a junction angle equal to 30^o and the diameter ratio equal to 1 corresponded to the optimal configuration.

The Constructal Law deals with the physical concepts of life, evolution, design, performance and time arrow (BEJAN, 2016). It states that "for a finite-size system to persist in time (to live), it must evolve in such a way that it provides easier access to the imposed currents that flow through it" (BEJAN, 1997). Constructal Design is the study and mathematical modeling of the evolution of flow systems. It is based on the Constructal Law and is a method to assess the effect of shape and geometry parameters on the performance of systems to provide easier access to the currents that flow through them (BEJAN and LORENTE, 2008; ROCHA et al., 2017).

2 METHODOLOGY

2.1 Arterial Bypass Graft Constructal Design

The geometry under investigation is an idealized version of an artery-bypass set previously employed by Dutra et al. (2020). The problem domain, dimensions and lines of further analysis are depicted in Fig. 1. The artery is the main tube with diameter D = 3 mm, as suggested by Bertolotti et al. (2001) to represent the average value of a right coronary human artery. The artery length is equal to L, the stenosis narrowest diameter is D_0 and L_5 and L_6 are the lengths to ensure fully developed flow. The bypass, with diameter D_1, is located at a distance L_2 from the center of the stenosis (D_0) and the junction angle is denoted as α. This model is shown in Fig. 1(a), with labels for lengths, diameters and positions used in this analysis. Figure 1(b) and Figure 1(c) show specific lines of analysis that are used herein (inner wall, outer wall and side wall lines). Table 1 summarizes the relative dimensions of this model. In these definitions, the work of Vimmr et al. (2012) was used as reference.

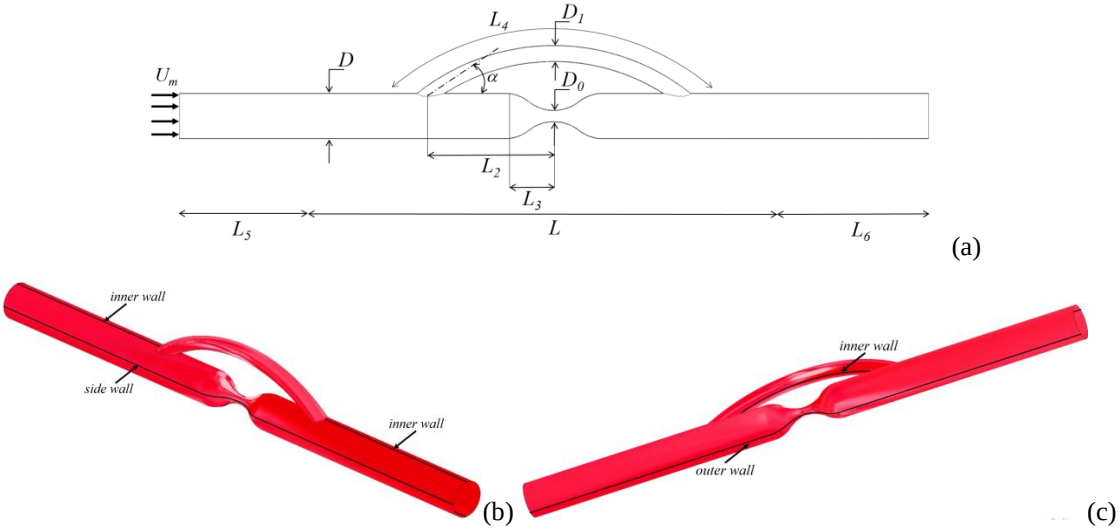

Figure 1 – Geometric model. (a) Domain dimensions. (b) Lines of analysis, inner and side walls. (c) Lines of analysis, inner and outer walls.

Table 1 – Relative dimensions for artery and graft build up.

Parameters	Values
L/D	16.67
L_2/D	2.5
L_3/D	1

The reference volume for this analysis is defined in Eq. (1)

$$\boldsymbol{V = \pi \frac{D^2}{4} L} \tag{1}$$

and the graft volume in Eq. (2)

$$V_1 = \pi \frac{{D_1}^2}{4} L_4 \tag{2}$$

where dimensions D_1 and L_4 have been defined in Fig. 1.

The stenosis degree is calculated with Eq. (3)

$$S = \frac{D - D_0}{D} x100\% \tag{3}$$

The flow under investigation is the steady-state, incompressible and laminar flow of blood which enters the domain with uniform velocity equal to U_m. A critical stenosis degree S

equal to 75% is evaluated at two different Reynolds numbers (150 and 250). Blood is modeled both as a Newtonian and a non-Newtonian shear-thinning fluid with the Carreau model (CARREAU, 1972).

Constructal Theory assumes that living systems evolve, limited by space, in the direction that provides easier access to the flows that consist in the purpose of such systems (BEJAN and LORENTE, 2008). The Constructal Design Method has been employed in other works following the method described in Fig. 2 (DOS SANTOS et al., 2017; ROCHA et al., 2017). A flow system must be defined as well as the type of flow and its magnitude in steps 1 and 2. In this case, the system is the set artery and the type of flow is steady-state blood flow. The 3rd step consists of defining a performance indicator that measures resistance to flow which is the design parameter to be minimized. In this case, the performance indicator is the pressure drop $\tilde{p}$ along the length L. The 4th and 5th steps define the constraints and degrees of freedom. In this system, the constraints are the set artery and bypass graft and their lengths, while the degrees of freedom are the junction angle, α, and the graft-artery diameter ratio (D_1/D). Step 6 is the numerical solution while the optimization of step 7 consists of a search for D_1/D and α that minimizes $\tilde{p}$ (denoted as $\tilde{p}_{min}$) for specific combinations of Carreau rheological parameters and Reynolds numbers. Newtonian and non-Newtonian outcomes were also compared with regards to the influence of each rheological parameter of the Carreau model for blood.

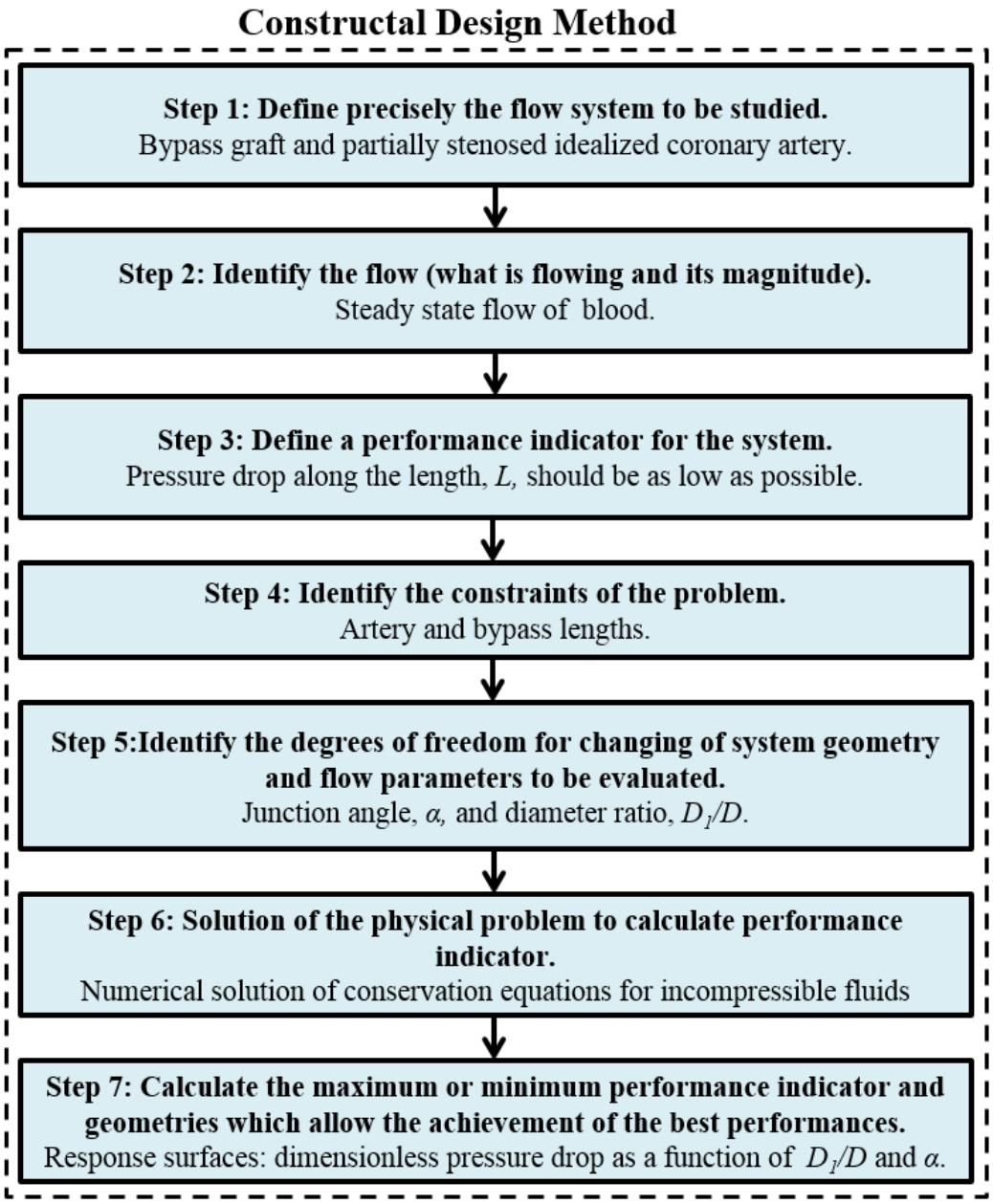

Figure 2 – Application of Constructal Design Method for the case studied.

2.2 MATHEMATICAL MODEL

The mathematical model for the flow through the system consists of the mass and momentum balance equations for incompressible flow. The dimensionless forms of these equations are given by Eq. (4) and Eq. (5), respectively

$$\frac{\partial \tilde{u}_i}{\partial \tilde{x}_i} = 0 \tag{4}$$

$$\tilde{u}_i \frac{\partial \tilde{u}_i}{\partial \tilde{x}_j} = -\frac{\partial \tilde{P}}{\partial \tilde{x}_i} + \frac{1}{Re}\frac{\partial \tilde{\tau}_{ij}}{\partial x_j} \quad (5)$$

where $\tilde{u}_i$ refers to the dimensionless velocity field; $\tilde{x}_i$ is the dimensionless position vector; $\tilde{P}$ is the dimensionless pressure; $\tilde{\tau}_{ij}$ is the dimensionless extra stress tensor; and Re is the Reynolds number. These parameters are defined in Eq. (6) as

$$\tilde{u}_i = \frac{u_i}{U_m}; \qquad \tilde{x}_i = \frac{x}{D}; \quad \tilde{P} = \frac{p}{\rho U_m^2}; \quad \tilde{\tau} = \frac{\tau_{ij}}{(U_m \eta_c)/D}; \qquad Re = \frac{\rho U_m D}{\eta_c} \quad (6)$$

where ρ is the mass density; U_m is the average inlet velocity and η_c is the characteristic viscosity.

The constitutive equation for the extra stress (τ_{ij}) is that of a generalized Newtonian liquid of Eq. (7)

$$\tau_{ij} = 2\eta(\dot{\gamma})D_{ij} \quad (7)$$

where $\eta(\dot{\gamma})$ is the viscosity as a function of the magnitude of the strain rate tensor (D_{ij}) (SLATTERY, 1999). Several authors, such as Cho and Kensey (1991), Johnston et al. (2004), Molla and Paul (2012), Pereira et al. (2013), Karimi et al. (2014), Fortuny et al. (2015), Doost et al. (2016), Iasiello et al. (2017) and Mehri et al. (2018) used the Carreau viscosity function (CARREAU, 1972) to model blood as a non-Newtonian shear-thinning fluid. The Carreau equation models viscosity as a function of shear rate in viscometric flows. The Carreau model predicts a high viscosity plateau (η_0) at low shear rates and a low viscosity plateau (η_∞) at high shear rates. A flow index (n) models the viscosity decay as the shear rate grows. In the case of non-viscometric and 3D flows, the Carreau function may be employed to represent the viscosity as a function of $\dot{\gamma}$, i.e., the magnitude of the strain rate tensor, as was the case in the present study. The Carreau viscosity function employed in the present study is shown in Eq. (8)

$$\eta(\dot{\gamma}) = \eta_\infty + (\eta_0 - \eta_\infty)(1 + (\lambda\dot{\gamma})^2)^{\frac{n-1}{2}} \quad (8)$$

where η_0 denotes the zero shear rate viscosity, η_∞ is the infinite shear rate viscosity, λ is the time constant, and n the flow index. The dimensionless form of this model is given by Eq. (9)

$$\tilde{\eta} = 1 + (\eta^* - 1)(1 + (\dot{\gamma}^*)^2)^{\frac{n-1}{2}} \quad (9)$$

and the dimensionless parameters of Eq. (9) are given by Eq. (10)

$$\tilde{\eta} = \frac{\eta(\dot{\gamma})}{\eta_\infty}; \qquad \eta^* = \frac{\eta_0}{\eta_\infty}; \qquad \dot{\gamma}^* = \frac{\dot{\gamma}}{\lambda} \quad (10)$$

where η_∞ was the characteristic viscosity of Eq. (6). Another dimensionless group that is important is the Carreau number (DE SOUZA MENDES, 2007) which represents a dimensionless version of the time constant in the Carreau equation given by Eq. (11)

$$\tilde{\lambda} = \frac{\lambda U_m}{D} \quad (11)$$

It should be noted that the same dimensionless group that accounts for fluid elasticity using characteristic time and characteristic shear rate is also commonly known as the "Weissenberg Number" (ASTARITA and MARRUCCI, 1974). In the present study, however, this dimensionless parameter is not related to elasticity but to the ratio of characteristic flow and fluid shear rates. The latter is the shear rate in which viscosity starts to drop due to shear-thinning. The physical interpretation of such a definition is that at higher Carreau numbers, the flow will be subjected to lower viscosities because the flow shear rates along the domain will be higher than that in which the viscosity starts to drop. If the Carreau number is high enough, the flow domain may be subjected to a viscosity equal to η_∞.

The result under analysis is the dimensionless pressure drop along the length *L* in Fig. 1 shown in Eq. (12)

$$\tilde{p} = \frac{\Delta p}{\rho U_m^2} \quad (12)$$

2.3 RHEOLOGICAL PARAMETERS

An extensive review was conducted to determine the rheological parameters used in previous studies with the Carreau fluid model for blood. Table 2 summarizes the main cases and their respective values.

Table 2 – Reference Carreau parameters used for blood.

Authors	η^*	λ	n	Hematocrit	Temperature
Cho and Kensey (1991)	16.2	3.313	0.3568	40%	-
Johnston et al. (2004)	16.2	3.313	0.3568	-	-
Molla and Paul (2012)	16.2	3.313	0.3568	-	-
Pereira et al. (2013)	14.3	3.313	0.3440	-	-
Pereira et al. (2013)	16.2	3.313	0.3568	-	-
Pereira et al. (2013)	7.1	25	0.2500	-	-
Karimi et al. (2014)	16.0	3.313	0.3568	40%	-
Fortuny et al. (2015)	16.2	3.313	0.3568	-	-
Doost et al. (2016)	16.0	3.313	0.3568	-	-
Iasiello et al. (2017)	16.2	3.313	0.3568	-	-
Mehri et al. (2018)	16.8	3.313	0.3530	5%	23°C
Mehri et al. (2018)	56.2	3.312	0.3690	10%	23°C
Mehri et al. (2018)	11.5	3.313	0.3520	5%	37°C
Mehri et al. (2018)	51.6	3.312	0.3620	15%	23°C
Mehri et al. (2018)	10.2	3.312	0.3530	10%	37°C
Mehri et al. (2018)	16.2	3.313	0.3560	45%	37°C
Mehri et al. (2018)	33.2	3.314	0.1520	15%	37°C

An important point is that only a few studies in Table 2 reported the percentage of hematocrit and only the experimental work by Mehri et al. (2018) collected the influence of hematocrit and temperature on blood parameters. Based on the data of Table 2, the present study selected extrapolated parameters for blood beyond the references in order to assess the effect of extreme behaviors on geometry performance and to verify the influence of each individual parameter in the Constructal Design. The extrapolated parameters are shown in Table 3.

Table 3 – Range of rheological parameters of the Carreau blood model.

Parameters	Values
η^*	15 – 1000
λ	3 – 50
n	0.35 – 0.60

2.4 NUMERICAL METHOD AND COMPUTATIONAL GRID

The present work applied the same numerical model and settings adopted in the previous work of Dutra et al. (2020), which employed the Finite Volume Method of Patankar (1980) in ANSYS/FLUENT v. 18.2 (ANSYS, 2015). The pressure-based solver with the pressure-velocity coupling method was employed, using second-order interpolation functions for pressure and velocity. All calculations were done using a double precision representation of real numbers. The iterative algorithm was a false transient. As a convergence criterion, the

scaled residuals of each equation at each iteration were compared with a user-defined convergence criterion equal to 10^{-6}. If the residual for each equation was less than the user-specified value, that equation was deemed to have converged for a time step. (ANSYS, 2015).

The mesh was parameterized to keep the element sizes proportional to the diameter ratio studied. Depending on the configuration, a total of 500,000 to 950,000 tetrahedral finite elements were necessary to mesh the computational domain accurately. Along the walls, prismatic layers elements were used to better capture the boundary layer. Figure 3 presents a sample of the computational mesh for the model with detailed views.

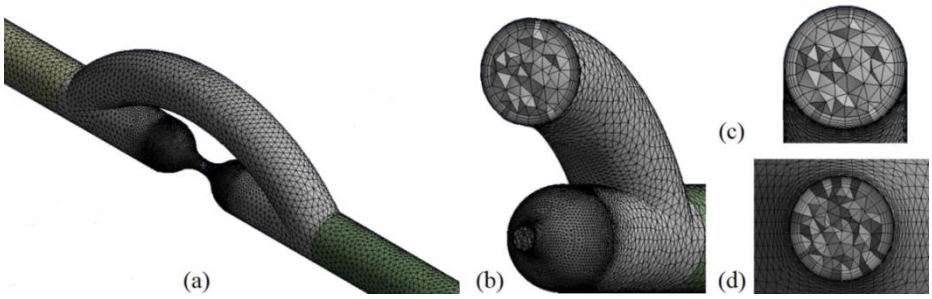

Figure 3 – Isometric view of the computational mesh for the model (a) with a view at the cross-section in the bypass and artery (b) and a front mesh view of the bypass (c) and stenosis region (d).

In a Dutra et al. (2020), a verification study was performed for this model. The *Grid Convergence Index (GCI)* method was applied for different values of junction angle (α) and diameter ratio (D_1/D) in three different values of stenosis degree (S = 25%, 50%, and 75%). Table 4 presents a comparison between the two higher *GCI* found for Newtonian blood and the respective *GCI* values for non-Newtonian blood in the same bypass configuration with N representing the number of elements. Thus, it can be verified that the maximum *GCI* for the non-Newtonian case is 1.14% when refining the mesh in the same factor of 15% to 30%. It is important to observe that a maximum GCI value of 5% is considered acceptable for this method (CELIK et al., 2008).

Table 4 – *Grid Convergence Index (GCI)* comparison for the Newtonian and non-Newtonian cases in the same bypass configurations at *Re = 250*.

	Newtonian Case 1	non-Newtonian Case 1	Newtonian Case 2	non-Newtonian Case 2
D_1/D	1	1	1	1
α	70°	70°	70°	70°
S	25%	25%	75%	75%
μ	0.0035	-	0.0035	-

η^*	-	15	-	15
λ	-	3	-	3
n	-	0.35	-	0.35
N1	510,872	510,872	803,049	803,049
N2	434,428	434,428	651,633	651,633
N3	368,760	368,760	490,328	490,328
$\tilde{p}_{,N1}$	2.362	2.641	3.924	4.107
$\tilde{p}_{,N2}$	2.415	2.601	3.928	4.097
$\tilde{p}_{,N3}$	2.437	2.598	3.929	4.036
GCI	**1.82%**	**1.14%**	**1.66%**	**1.12%**

The response surface methodology available in ANSYS Design Xplorer 18.2 (ANSYS, 2016) was applied to investigate the effects of α and D_1/D on pressure drop along the length L. A sparse grid method (MONTGOMERY, 2013) was adopted to build the response surfaces and represent $\tilde{p}$ as a function of the degrees of freedom D_1/D and α. Sparse Grid is an adaptive model driven by the accuracy defined by the user. Initially, the program calculated four design points located at the edges and one design point located at the center of the response surface. Then, the response surface was elaborated with a maximum number of 1,000 design points per surface. It is noteworthy that each design point represented a specific bypass configuration within the ranges $0.1 \leq D_1/D \leq 1.0$ and $30^o \leq \alpha \leq 70^o$. In this study, the number of points needed to construct each surface ranged from 200 to 300.

3 RESULTS AND DISCUSSION

3.1 RESPONSE SURFACES

Eighteen response surfaces were generated by the sparse grid method (MONTGOMERY, 2013). Figure 4 presents a comparison between two samples of response surfaces that represent $\tilde{p}$ as a function of D_1/D and α. Figure 4(a) represents the Newtonian case (μ = 0.0035 Pa.s / η^* = 1) while Fig. 4(b) exhibits the non-Newtonian baseline case (η^* = 15; λ = 3; n = 0.35). Both response surfaces represent the results of stenosis degree S of 75% at a Reynolds number of 150.

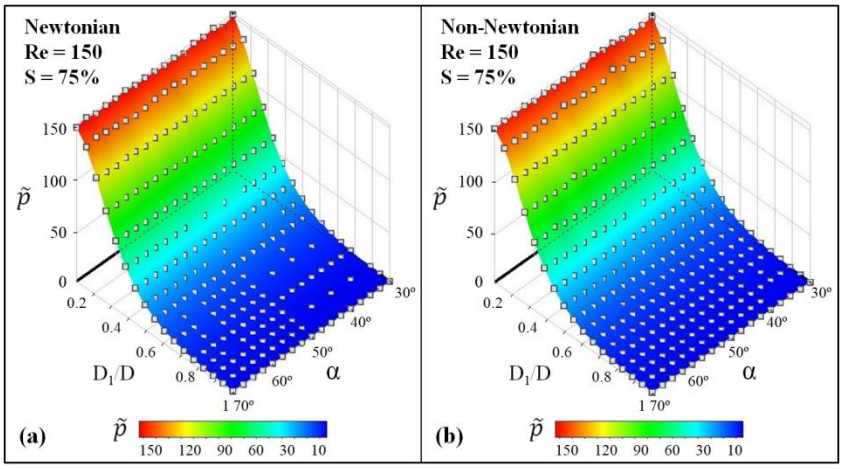

Figure 4 – Response surfaces representing $\tilde{p}$ as a function of D_1/D and α for the stenosis degree equal to 75% and Reynolds number equal to 150: (a) Newtonian case (μ = 0.0035 Pa.s); (b) non-Newtonian baseline case (η^* = 15; λ = 3; n = 0.35).

Following the same trend of Fig. 4, a high similarity was seen in all the response surfaces generated for the Newtonian and non-Newtonian cases. In Fig. 4, it is possible to observe that both response surfaces had a specific optimal combination point of D_1/D and α that minimized the dimensionless pressure drop ($\tilde{p}$). In all situations $\tilde{p}$ decreased as the aspect ratio D_1/D increased to 1 and the junction angle α decreased to 30º. As the flow was highly deviated through the bypass, the influence of α in $\tilde{p}$ became almost unnoticeable.

Tables 5 and 6 summarize the optimal geometry results for the eighteen configurations. The parameter λ is represented in the table by the Carreau number ($\tilde{\lambda}$) which varies the value of λ in the viscosity function (ZINANI and FREY, 2008). It is possible to notice a considerable dependence of $\tilde{p}$ on rheological parameters, especially η^* and n. Also, the optimum point for all cases was a $D_1/D_{,opt}$ ratio equal to 1 and $\alpha_{,opt}$ equal to 30°.

Table 5 – Optimum results for stenosis degree equal to 75%, at *Re* equal to 150.

Re	*Case*	μ	η^*	λ	$\tilde{\lambda}$	n	$\tilde{p}_{,\min}$	$D_1/D_{,\text{opt}}$	$\alpha_{,\text{opt}}$
	Newtonian	0.0035	1	-	-	-	3.978	1	30°
	Non-Newtonian	-	15	3	175	0.35	4.472	1	30°
	Non-Newtonian	-	15	3	175	0.60	6.750	1	30°
	Non-Newtonian	-	15	50	2916.7	0.35	4.054	1	30°
150	Non-Newtonian	-	15	50	2916.7	0.60	4.853	1	30°
	Non-Newtonian	-	1000	3	175	0.35	38.237	1	30°
	Non-Newtonian	-	1000	3	175	0.60	207.53	1	30°
	Non-Newtonian	-	1000	50	2916.7	0.35	9.517	1	30°
	Non-Newtonian	-	1000	50	2916.7	0.60	69.217	1	30°

Table 6 – Optimum results for stenosis degree equal to 75%, at *Re* equal to 250.

Re	*Case*	μ	η^*	λ	$\tilde{\lambda}$	n	$\tilde{p}_{,\min}$	$D_1/D_{,opt}$	$\alpha_{,opt}$
	Newtonian	0.0035	1	-	-	-	2.659	1	30°
	Non-Newtonian	-	15	3	291.7	0.35	2.866	1	30°
	Non-Newtonian	-	15	3	291.7	0.60	3.992	1	30°
	Non-Newtonian	-	15	50	4861.1	0.35	2.710	1	30°
250	Non-Newtonian	-	15	50	4861.1	0.60	3.091	1	30°
	Non-Newtonian	-	1000	3	291.7	0.35	17.621	1	30°
	Non-Newtonian	-	1000	3	291.7	0.60	103.93	1	30°
	Non-Newtonian	-	1000	50	4861.1	0.35	5.238	1	30°
	Non-Newtonian	-	1000	50	4861.1	0.60	35.444	1	30°

For the two Reynolds numbers studied, the Newtonian case resulted in the lowest value of the dimensionless pressure drop. This finding suggests that the choice of assuming Newtonian behavior to blood may underestimate the value of pressure drop in the system. For the Newtonian case (μ = 0.0035 Pa.s) and the non-Newtonian baseline case (η^* = 15; λ = 3; n = 0.35) of this study, the underestimation was of about 12.4% for *Re = 150* and 7.8% for *Re* = 250. Weddell et al. (2015) reached the same result in a pulsating study of an artery tree, where the Newtonian pressure drop found was lower than the non-Newtonian one. However, the differences in Weddell et al. (2015) ranged from 31% to 133% depending on the time lapse analyzed. The difference with respect to this study can be explained by the geometry analyzed and flow regime adopted.

Even so, the results obtained demonstrated that non-Newtonian rheological parameters influenced neither the shape of the response surfaces nor the optimum points found. In the previous study of Dutra et al. (2020), the same optimum point was found for different stenosis degrees (*S*) equal to 25%, 50%, and 75% at three different Reynolds numbers. Likewise, these discoveries were in line with the work of Abraham et al. (2005), who verified no significant differences in the optimal junction angle obtained using Newtonian and non-Newtonian models. More recently, Vimmr et al. (2013) suggested that the bypass diameter was a more important parameter than the application of a non-Newtonian model. Furthermore, it was asserted that the diameter was the main determinant parameter for the patency and overall performance of a bypass graft.

3.2 VELOCITY FIELDS AND STREAMLINES

Velocity field data are presented in Fig. 5 for the optimum junction angle ($\alpha_{,opt}$ = 30°) and diameter ratio ($D_1/D_{,opt}$ = 1) shown in Table 5 at *Re* = 150 and *S* = 75%. The Newtonian case and four specific non-Newtonian cases are shown with the main focus on the effect provided by the variation of rheological parameters.

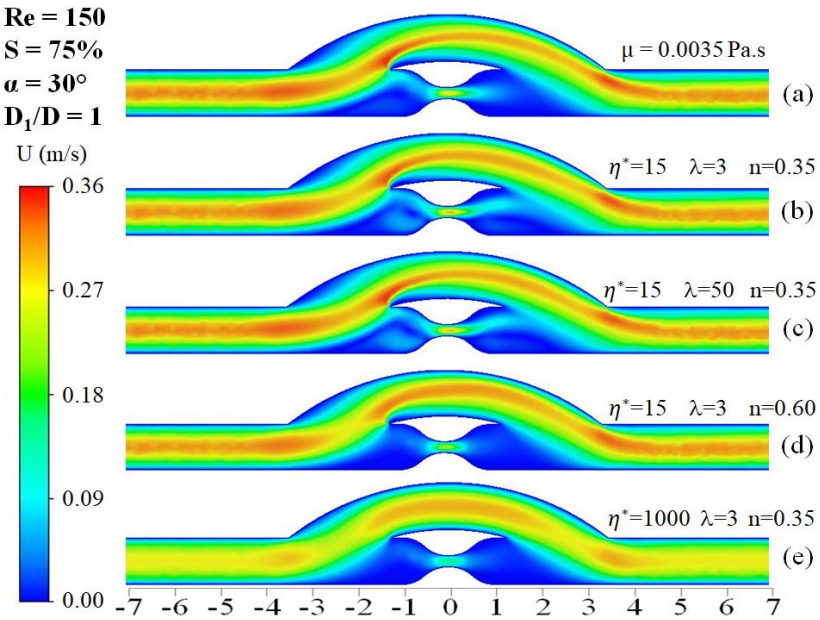

Figure 5 – Effect provided by the variation of rheological parameters in the optimum junction angle, $\alpha_{,opt}$ = 30° and diameter ratio, $D_1/D_{,opt}$ = 1, at velocity contours for stenosis degree, *S* = 75% and *Re* = 150. Newtonian case (a) μ = 0.0035 Pa.s; and non-Newtonian cases (b) η^*=15; λ=3; *n*=0.35; (c) η^*=15; λ=50; *n*=0.35; (d) η^*=15; λ=3; *n*=0.60; (e) η^*=1000; λ=3; *n*=0.35.

In general, the first three bypasses of Fig. 5(a-c) present a similar velocity field, while the last two of Fig. 5(d-e) differ from the others. This velocity field behavior can be explained by the variation of the blood rheological parameters η^* and *n*, which appears to have a more pronounced influence on the velocity field than λ. The most significant change in flow can be noted for the highest η^* value of Fig. 5(e). This is explained by the greater drop in viscosity that occurred in this case between the η_0 and η_∞ plateaus. For lower η^* values, as are the cases of Fig. 5(a-d), the drop in viscosity does not cause noticeable changes in the flow.

Also, it is possible to assert that, by decreasing the bypass diameter, the non-Newtonian effects on the flow could become more relevant because the shear rate would increase with the reduction in diameter and cause a drop in blood viscosity. Nonetheless, as demonstrated in the previous study of Dutra et al. (2020), smaller diameters caused a higher pressure drop, which was not desired for the bypass performance.

Besides, with the variation of blood parameters, it is possible to note different flow zones in the region upstream of stenosis ($\tilde{x}$ = -2 to 0) of Fig. 5. Other changes occur in the stenosis region ($\tilde{x}$ = 0), where the shear-thinning characteristics of blood affect the jet flow. It is noteworthy that this phenomenon occurs due to the increase in the shear stress caused by the sudden reduction in the diameter of the artery (stenosis). Sood et al. (2018) analyzed the complexity of these patterns in non-Newtonian blood flow through axisymmetric and asymmetric stenosis and in the post stenotic region. However, the role of this phenomenon as a pathological determinant is still debatable (ANDERSSON et al., 2019).

Streamlines were generated to visualize the differences in the regions upstream ($\tilde{x}$ = -2 to 0) and downstream ($\tilde{x}$ = 0 to 2) of stenosis. Results are shown in Fig. 6 under the same flow configurations.

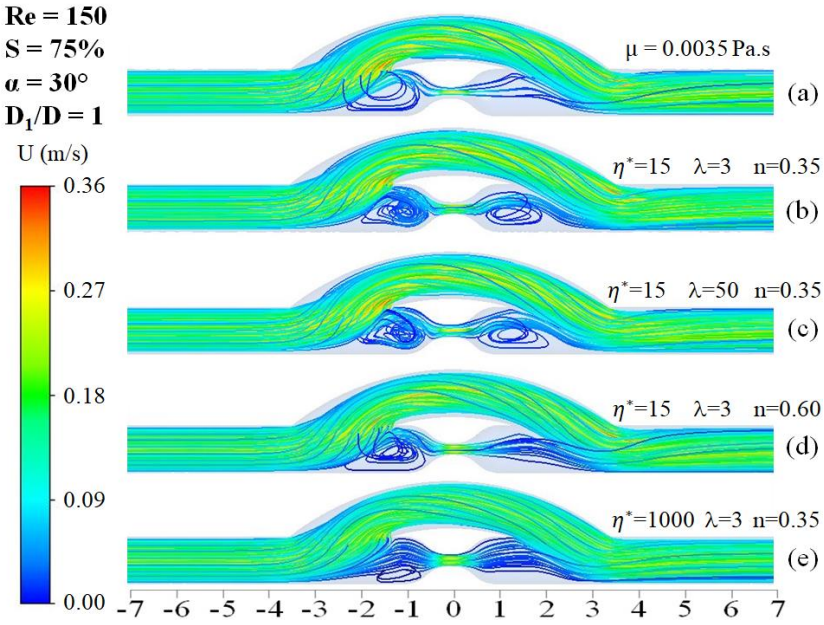

Figure 6 – Effect provided by the variation of rheological parameters in the optimum junction angle, $\alpha_{,opt}$ = 30° and diameter ratio, $D_1/D_{,opt}$ = 1, at streamlines for stenosis degree, S = 75% and Re = 150. Newtonian case (a) μ = 0.0035 Pa s; and non-Newtonian cases (b) η^*=15; λ=3; n=0.35; (c) η^*=15; λ=50; n=0.35; (d) η^*=15; λ=3; n=0.60; (e) η^*=1000; λ=3; n=0.35.

Figure 6(a-e) highlights that larger recirculation zones appear in all bypasses in the region upstream of stenosis, while only Fig. 6(b-c) presents this phenomenon downstream of stenosis. As previously shown in Fig. 5(d-e), these last two cases differ from the others due to the variation of rheological parameters and shear-thinning effects. Vimmr and Jonášová (2010) also observed differences in velocity distribution and profile.

The appearance of recirculation zones is especially important downstream of stenosis, where the occurrence of intimal hyperplasia is known to be more prevalent. This finding

demonstrates the importance of choosing a non-Newtonian fluid model for blood because the choice of a Newtonian model may underestimate this phenomenon. This situation was already well reported by several studies. Bertolotti et al. (2001), Lee et al. (2001) and Ko et al. (2007) observed the same recirculation zones in the regions upstream and downstream of stenosis and concluded that these zones were two critical locations where the blood cells could be damaged and tended to accumulate. Thus, these studies demonstrated the influence of recirculation zones on bypass failure. Chen et al. (2006) concluded that a Newtonian model for blood might lead to false conclusions, especially in complex vascular geometries. O´Callaghan et al. (2006) stated that blood could not be treated as a Newtonian or non-Newtonian fluid in general and under all situations. Instead, it was considered more useful to consider each case individually depending on which configuration was investigated. Vimmr and Jonášová (2010) studied a femoral bypass and observed several underestimated recirculation zones, especially before the occlusion, and indicated that blood non-Newtonian behavior was particularly evident in the post stenotic region.

As cited from other studies, non-uniform hemodynamics is well recognized for contributing to restenosis and the blood cells accumulation. So, the findings of this study demonstrate the importance of choosing a non-Newtonian fluid model for blood because the choice of a Newtonian model may underestimate the recirculation phenomenon.

3.3 WALL SHEAR STRESS (WSS)

The shear stress behavior at the artery wall caused by the variation of rheological parameters of the blood was analyzed at *Re* of 150 and stenosis degree *S* of 75%. The shear stress found at each point was normalized by the shear stress found in the fully developed condition of the artery. Figures 7 through 9 present the results of WSS at lines located along the artery wall as depicted in Fig. 1(b-c), namely inner, outer, and side wall lines. Along the three wall lines, it was possible to observe that higher normalized WSS values were obtained in the constricted area ($\tilde{x}$ = 0) for the Newtonian case (μ = 0.0035 Pa.s) and the non-Newtonian baseline case (η^* = 15; λ = 3; n = 0.35). A less representative increase in normalized WSS occurred in the same region for other non-Newtonian configurations.

Figure 7 shows that along the inner wall the Newtonian case (μ = 0.0035 Pa.s) and the non-Newtonian baseline case (η^* = 15; λ = 3; n = 0.35) induced higher normalized WSS values at the bypass entrance ($\tilde{x}$ = -2 to -1) and toe region ($\tilde{x}$ = 3 to 4). Also, in agreement with the results of Section 3.2, it is important to point out the presence of negative values of WSS in the

recirculation zones near stenosis ($\tilde{x}$ = -1 to 0 and $\tilde{x}$ = 0 to 1). Chen et al. (2006) also observed flow recirculation in the post stenotic region near the inner wall and higher values of WSS in all cases near the heel.

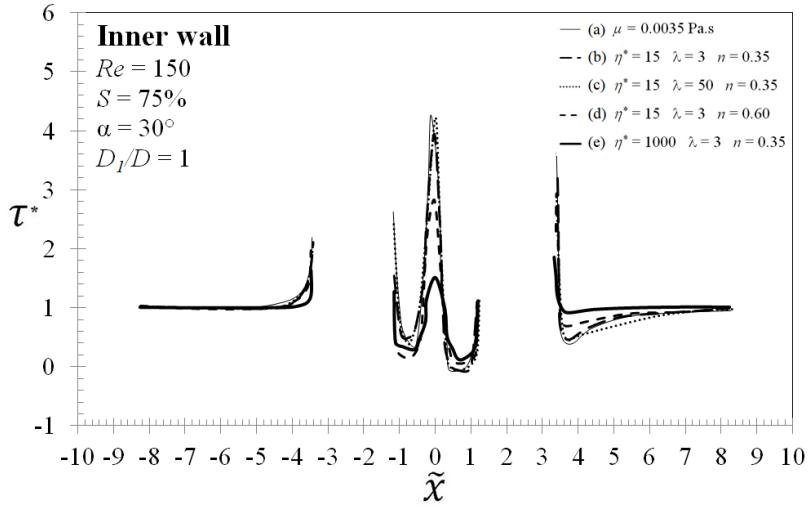

Figure 7 – Results of normalized shear stress, τ^*, on the inner wall provided by the variation of rheological parameters in the optimum junction angle, $\alpha_{,opt}$ = 30° and diameter ratio, $D_1/D_{,opt}$ = 1, for stenosis degree, S = 75% and Re = 150. Newtonian case (a) μ = 0.0035 Pa.s; and non-Newtonian cases (b) η^*=15; λ=3; n=0.35; (c) η^*=15; λ=50; n=0.35; (d) η^*=15; λ=3; n=0.60; (e) η^*=1000; λ=3; n=0.35.

At the outer wall (Fig. 8) and sidewall (Fig. 9), a high similarity between Newtonian and non-Newtonian results is observed. In both cases, the most remarkable occurrence is the presence of negative values of WSS in the recirculation zones near stenosis ($\tilde{x}$ = -1 to 0 and $\tilde{x}$ = 0 to 1) and a shear stress peak in the artery bed ($\tilde{x}$ = 3 to 4). It is important to observe that the results for the Newtonian and three non-Newtonian cases have similar behavior, except for the non-Newtonian case with higher η^* = 1000 of Fig. 8(e) and 9(e). These are also explained by the higher drop in the viscosity curve that occurred between the η_0 plateau and the η_∞ plateau. Vimmr et al. (2013) asserted that the most significant changes in WSS were very specific and observed mainly in the upstream stenosis region, i.e., in unimportant areas to the intimal hyperplasia occurrence.

It is noteworthy that the WSS values shown in Fig. 7 through 9 have been normalized by the shear stress found in the fully developed condition in the artery. This procedure meant that the nominal WSS values for each case were quantitatively very different, especially for higher η^* values. In this point of view, O´Callaghan et al. (2006) stated that the results between Newtonian and non-Newtonian blood were qualitatively but not quantitatively similar and this situation should be considered when different works are compared.

Finally, it is important to emphasize that the major differences in WSS appeared only in the extrapolated values, i.e., on the non-Newtonian case with higher η^* = 1000. As already pointed out in Section 2.3 these values were adopted in order to assess if extreme behaviour could have important effects on geometry performance. Thus, it can be assumed that the adoption of a non-Newtonian model for blood does not significantly alter the WSS values in the study of a bypass graft

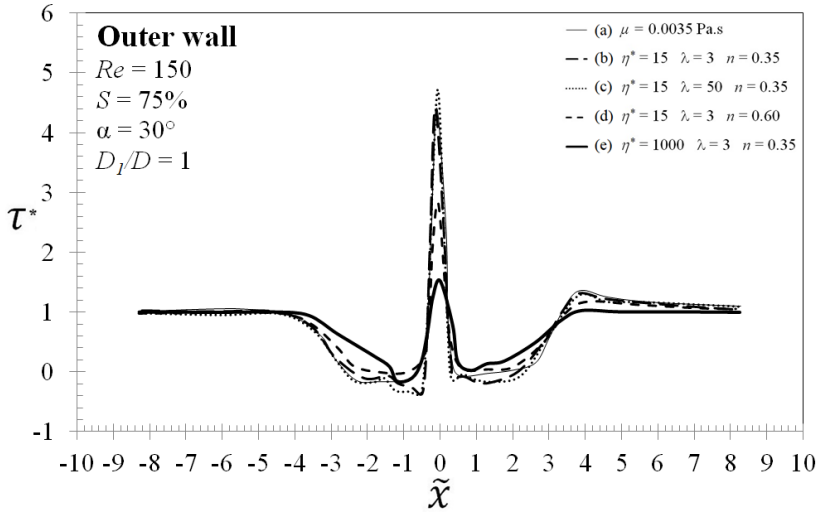

Figure 8 – Results of normalized shear stress, τ^*, on the outer wall provided by the variation of rheological parameters in the optimum junction angle, $\alpha_{,opt}$ = 30° and diameter ratio, $D_1/D_{,opt}$ = 1, for stenosis degree, S = 75% and Re = 150. Newtonian case (a) μ = 0.0035 Pa.s; and non-Newtonian cases (b) η^*=15; λ=3; n=0.35; (c) η^*=15; λ=50; n=0.35; (d) η^*=15; λ=3; n=0.60; (e) η^*=1000; λ=3; n=0.35.

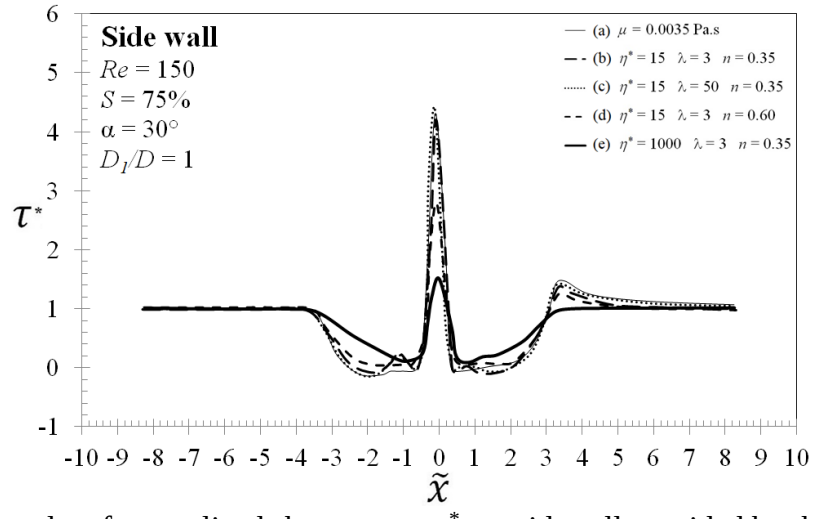

Figure 9 – Results of normalized shear stress, τ^*, on sidewall provided by the variation of rheological parameters in the optimum junction angle, $\alpha_{,opt}$ = 30° and diameter ratio, $D_1/D_{,opt}$ = 1, for stenosis degree, S = 75% and Re = 150. Newtonian case (a) μ = 0.0035 Pa.s; and non-Newtonian cases (b) η^*=15; λ=3; n=0.35; (c) η^*=15; λ=50; n=0.35; (d) η^*=15; λ=3; n=0.60; (e) η^*=1000; λ=3; n=0.35.

4 CONCLUSIONS

In this work, the effects of rheological parameters in different blood flow conditions of a bypass graft were investigated. A CFD model associated with Constructal Design and Sparse Grid method generated eighteen response surfaces, each one representing results for a severe stenosis degree of 75% for specific combinations of Carreau rheological parameters at two different Reynolds numbers of 150 and 250. The Newtonian and non-Newtonian outcomes were compared through an analysis of the influence of each rheological parameter of the Carreau model.

All the response surfaces generated for Newtonian and non-Newtonian cases presented a significant similarity, i.e., the dimensionless pressure drop ($\tilde{p}$) was minimized for D_1/D equal to 1 and α equal to 30º. This was in agreement with the previous study of Dutra et al. (2020) which determined the same optimal geometry for three different stenosis degrees S (25%, 50%, and 75%) at three different Reynolds Numbers (150, 250 and 400). However, in the present study, the dimensionless pressure drop was strongly dependent on rheological parameters. For the two Reynolds numbers studied, the Newtonian case presented the lowest value of the dimensionless pressure drop, which suggested that the choice of applying Newtonian blood may underestimate the value of pressure drop in the system. Even so, the results demonstrated that rheological parameters influenced neither the shape of the response surfaces nor the optimal geometry.

The effects of rheological parameters on velocity fields and wall shear stress (WSS) were also investigated. Parameters η^* and n had more pronounced influences on velocity, streamlines and recirculation zones than λ. Rheological parameters also resulted in the occurrence of recirculation zones, especially downstream of stenosis, where the occurrence of intimal hyperplasia is known to be more prevalent. On WSS, it should be stressed that the results for the Newtonian and most non-Newtonian cases had similar behavior, the exception being the non-Newtonian case with higher η^* value which was explained by the more significant drop in viscosity curve that occurred in this case.

At this point, some limitations of this study should be mentioned. First of all, a steady-state condition was applied while blood flow is known to be pulsating. Moreover, the grafts and arteries were assumed as rigid walls and idealized without considering a patient-specific vascular model. Also, there are limited experimental data available in reference studies that are essential for validation and clinical adoption of any proposed configuration. Despite these

simplifications and assumptions, by applying the Constructal Design methodology, the main conclusions and the optimal graft design found in this paper agree with previous Newtonian and non-Newtonian studies that evaluated graft design with the same and other methodologies.

ACKNOWLEDGEMENTS

Financial support for author R.F. Dutra was provided by the Unisinos Office of Research and Graduate Studies (UAPPG) and CAPES. Authors F.S.F. Zinani and L.A.O. Rocha were supported by CNPq grant process numbers 307827/2018-6 and 307791/2019-0, respectively, while author C. Biserni was sponsored by the Italian Ministry for Education, University and Research.

REFERENCES

ABRAHAM, F.; BEHR, M.; HEINKENSCHLOSS, M. Shape Optimization in Stationary Blood Flow: A Numerical Study of Non-Newtonian Effects. **Computer Methods in Biomechanics and Biomedical Engineering**, v. 8, p. 127–137, 2005. <http://dx.doi.org/10.1080/10255840500309562>

ANDERSSON, Magnus; EBBERS, Tino; KARLSSON, Matts. Characterization and estimation of turbulence-related wall shear stress in patient-specific pulsatile blood flow. **Journal of Biomechanics**, v. 85, p. 108–117, 2019. <https://doi.org/10.1016/j.jbiomech.2019.01.016>

ANSYS. **Ansys Fluent User's Guide**. Canonsburg, 2015.

ANSYS. **Design Xplorer User's Guide. Release 17.2**. Canonsburg, 2016.

APOSTOLIDIS, Alex J.; MOYER, Adam P.; BERIS, Antony N. Non-Newtonian effects in simulations of coronary arterial blood flow. **Journal of Non-Newtonian Fluid Mechanics**, v. 233, p. 155–165, 2016. <http://dx.doi.org/10.1016/j.jnnfm.2016.03.008>

ASTARITA, G.; MARRUCCI, G. **Principles of Non-Newtonian Fluid Mechanics**. Mcgraw-Hill, New York, 1974.

BASSIOUNY, Hisham S.; WHITE, Scott; GLAGOV, Seymour; CHOI, Eric; GIDDENS, Don P.; ZARINS, Christopher K. Anastomotic intimal hyperplasia: Mechanical injury or flow induced. **Journal of Vascular Surgery**, v. 15, n. 4, p. 708–717, 1992. <https://doi.org/10.1067/mva.1992.33849>

BEJAN, A. **Advanced Engineering Thermodynamics**. 2 ed, Wiley, New York, 1997.

BEJAN, A; LORENTE, S. **Design with Constructal Theory**. Wiley, Hoboken, 2008.

BEJAN, A. **The Physics of Life**, St. Martin's Press, New York, 2016.

BERTOLOTTI, C.; DEPLANO, V.; FUSERI, J.; DUPOUY, P. Numerical and experimental models of post-operative realistic flows in stenosed coronary bypasses. **Journal of Biomechanics**, v. 34, n. 8, p. 1049–1064, 2001. <https://doi.org/10.1016/S0021-9290(01)00027-6>

BODNÁR, T.; SEQUEIRA, A.; PROSI, M. On the shear-thinning and viscoelastic effects of blood flow under various flow rates. **Applied Mathematics and Computation**, v. 217, n. 11, p. 5055–5067, 2011. <http://dx.doi.org/10.1016/j.amc.2010.07.054>

BRUN, Jean Frédéric; VARLET-MARIE, Emmanuelle; CASSAN, Delphine; RAYNAUD DE MAUVERGER, Eric. Blood rheology and body composition as determinants of exercise performance in female rugby players. **Clinical Hemorheology and Microcirculation**, v. 49, n. 1–4, p. 207–214, 2011. <http://dx.doi.org/10.3233/CH-2011-1470>

BRUN, Jean Frédéric; VARLET-MARIE, Emmanuelle; FÉDOU, Christine; RAYNAUD DE MAUVERGER, Eric. One-year follow-up of blood viscosity factors and hematocrit/viscosity ratio in elite soccer players. **Clinical Hemorheology and Microcirculation**, v. 64, n. 4, p. 799–808, 2016. <http://dx.doi.org/10.3233/CH-168014>

CARREAU, Pierre J. Rheological Equations From Molecular Network Theories. **Transactions of the Society of Rheology**, v. 16, n. 1, p. 99–127, 1972. <https://doi.org/10.1122/1.549276>

CELIK, I. B.; GHIA, U.; ROACHE, P. J.; FREITAS, C. J.; COLEMAN, H.; RAAD, P. E. Procedure for Estimation and Reporting of Uncertainty Due to Discretization in CFD Applications. **Journal of Fluids Engineering**, v. 130, p. 128–131, 2008.

CHEN, Jie; LU, Xi Yun; WANG, Wen. Non-Newtonian effects of blood flow on hemodynamics in distal vascular graft anastomoses. **Journal of Biomechanics**, v. 39, n. 11, p. 1983–1995, 2006. <http://dx.doi.org/10.1016/j.jbiomech.2005.06.012>

CHO, Y. I.; KENSEY, K. R. Effects of the non-Newtonian viscosity of blood on flows in a diseased arterial vessel. Part 1: Steady flows. **Biorheology**, v. 28, n. 3–4, p. 241–262, 1991. <http://dx.doi.org/10.3233/BIR-1991-283-415>

DE SOUZA MENDES, Paulo R. Dimensionless non-Newtonian fluid mechanics. **Journal of Non-Newtonian Fluid Mechanics**, v. 147, n. 1–2, p. 109–116, 2007. <https://doi.org/10.1016/j.jnnfm.2007.07.010>

DOOST, Siamak N.; ZHONG, Liang; SU, Boyang; MORSI, Yosry S. The numerical analysis of non-Newtonian blood flow in human patient-specific left ventricle. **Computer Methods and Programs in Biomedicine**, v. 127, p. 232–247, 2016. <http://dx.doi.org/10.1016/j.cmpb.2015.12.020>

DOS SANTOS, E. D. et al. The Constructal Design Applied to Renewable Energy Systems. In: Sustainable Energy Technologies. [s.l.] CRC Press, 2017. p. 45–62.

DUTRA, R. F.; ZINANI, F. S. F.; ROCHA, L. A. O.; BISERNI, C. Constructal design of an arterial bypass graft**. Heat Transfer**, p. 1–21, 2020.<http://dx.doi.org/10.1002/htj.21693>

FORTUNY, Gerard; HERRERO, Joan; PUIGJANER, Dolors; OLIVÉ, Carme; MARIMON, Francesc; GARCIA-BENNETT, Josep; RODRÍGUEZ, Daniel. Effect of anticoagulant treatment in deep vein thrombosis: A patient-specific computational fluid dynamics study. **Journal of Biomechanics**, v. 48, n. 10, p. 2047–2053, 2015. <http://dx.doi.org/10.1016/j.jbiomech.2015.03.026>

GIJSEN, F. J. H.; ALLANIC, E.; VAN DE VOSSE, F. N.; JANSSEN, J. D. The influence of the non-Newtonian properties of blood on the flow in large arteries: Unsteady flow in a 90° curved tube. **Journal of Biomechanics**, v. 32, n. 7, p. 705–713, 1999. <http://dx.doi.org/10.1016/S0021-9290(99)00014-7>

GUIRAUDOU, Marie; VARLET-MARIE, Emmanuelle; RAYNAUD DE MAUVERGER, Eric; BRUN, Jean Frédéric. Obesity-related increase in whole blood viscosity includes different profiles according to fat localization. **Clinical Hemorheology and Microcirculation**, v. 55, n. 1, p. 63–73, 2013. <http://dx.doi.org/10.3233/CH-131690>

HORNER, Jeffrey S.; ARMSTRONG, Matthew J.; WAGNER, Norman J.; BERIS, Antony N. Investigation of blood rheology under steady and unidirectional large amplitude oscillatory shear. **Journal of Rheology**, v. 62, n. 2, p. 577–591, 2018. <https://doi.org/10.1122/1.5017623>

IASIELLO, Marcello; VAFAI, Kambiz; ANDREOZZI, Assunta; BIANCO, Nicola. Analysis of non-Newtonian effects within an aorta-iliac bifurcation region. **Journal of Biomechanics**, v. 64, p. 153–163, 2017. <https://doi.org/10.1016/j.jbiomech.2017.09.042>

JOHNSTON, Barbara M.; JOHNSTON, Peter R.; CORNEY, Stuart; KILPATRICK, David. Non-Newtonian blood flow in human right coronary arteries: Steady state simulations. **Journal of Biomechanics**, v. 37, n. 5, p. 709–720, 2004. <http://dx.doi.org/10.1016/j.jbiomech.2003.09.016>

KARIMI, Safoora; DABAGH, Mahsa; VASAVA, Paritosh; DADVAR, Mitra; DABIR, Bahram; JALALI, Payman. Effect of rheological models on the hemodynamics within human aorta: CFD study on CT image-based geometry. **Journal of Non-Newtonian Fluid Mechanics**, v. 207, p. 42–52, 2014. <http://dx.doi.org/10.1016/j.jnnfm.2014.03.007>

KIM, Ji Tae; SUNG, Kun Hyuk; RYOU, Hong Sun. A numerical study on the effect of hematocrit on hemodynamic characteristics in arteriovenous graft. **Korea Australia Rheology Journal**, v. 26, n. 3, p. 327–334, 2014. <http://dx.doi.org/10.1007/s13367-014-0037-x>

KO, T. H.; TING, K.; YEH, H. C. Numerical investigation on flow fields in partially stenosed artery with complete bypass graft: An in vitro study. **International Communications in Heat and Mass Transfer**, v. 34, n. 6, p. 713–727, 2007. <http://dx.doi.org/10.1016/j.icheatmasstransfer.2007.03.010>

LEE, D.; SU, J. M.; LIANG, H. Y. A numerical simulation of steady flow fields in a bypass tube. **Journal of Biomechanics**, v. 34, n. 11, p. 1407–1416, 2001.

https://doi.org/10.1016/S0021-9290(01)00131-2

MARCINKOWSKA-GAPIŃSKA, Anna; GAPINSKI, Jacek; ELIKOWSKI, Waldemar; JAROSZYK, Feliks; KUBISZ, Leszek. Comparison of three rheological models of shear flow behavior studied on blood samples from post-infarction patients. **Medical and Biological Engineering and Computing**, v. 45, n. 9, p. 837–844, 2007. <http://dx.doi.org/10.1007/s11517-007-0236-4>

MEHRI, Rym; MAVRIPLIS, Catherine; FENECH, Marianne. Red blood cell aggregates and their effect on non-Newtonian blood viscosity at low hematocrit in a two-fluid low shear rate microfluidic system. **PLoS ONE**, v. 13, n. 7, 2018. <http://dx.doi.org/10.1371/journal.pone.0199911>

MOLLA, M. M.; PAUL, M. C. LES of non-Newtonian physiological blood flow in a model of arterial stenosis. **Medical Engineering and Physics**, v. 34, n. 8, p. 1079–1087, 2012. <https://doi.org/10.1016/j.medengphy.2011.11.013 >

MONTGOMERY, D.C. **Design and Analysis of Experiments**, 8. ed., John Wiley & Sons, New Jersey, 2013.

O'CALLAGHAN, Siobhan; WALSH, Michael; MCGLOUGHLIN, Timothy. Numerical modelling of Newtonian and non-Newtonian representation of blood in a distal end-to-side vascular bypass graft anastomosis. **Medical Engineering and Physics**, v. 28, p. 70–74, 2006. <http://dx.doi.org/10.1016/j.medengphy.2005.04.001>

OWENS, Robert G. A new microstructure-based constitutive model for human blood. **Journal of Non-Newtonian Fluid Mechanics**, v. 140, n. 1–3, p. 57–70, 2006. <http://dx.doi.org/10.1016/j.jnnfm.2006.01.015>

PATANKAR, S. V. **Numerical Heat Transfer and Fluid Flow**. McGraw-Hill, New York, 1980.

PEREIRA, J. M. C.; SERRA E MOURA, J.P.; ERVILHA, A.R.; PEREIRA, J.C.F. On the uncertainty quantification of blood flow viscosity models. **Chemical Engineering Science**, v. 101, p. 253–265, 2013. <http://dx.doi.org/10.1016/j.ces.2013.05.033>

RAZAVI, A.; SHIRANI, E.; SADEGHI, M. R. Numerical simulation of blood pulsatile flow in a stenosed carotid artery using different rheological models. **Journal of Biomechanics**, v. 44, n. 11, p. 2021–2030, 2011. <http://dx.doi.org/10.1016/j.jbiomech.2011.04.023>

ROCHA, L. A. O.; LORENTE, S.; BEJAN, A. Constructal Theory in Heat Transfer. In: KULACKI F. **Handbook of Thermal Science and Engineering.** Springer, 2017. Chap. 1, p. 1-32. <https://doi.org/10.1007/978-3-319-32003-8_66-1>

SAEDI ARDAHAIE, S.; JAFARIAN AMIRI, A.; AMOUEI, A.; HOSSEINZADEH, K.; GANJI, D.D. Investigating the effect of adding nanoparticles to the blood flow in presence of magnetic field in a porous blood arterial. **Informatics in Medicine Unlocked**, v. 10, p. 71-81, 2018. <https://doi.org/10.1016/j.imu.2017.10.007>

SLATTERY, J., C. **Advanced Transport Phenomena**. Cambridge University Press, New York, 1999.

SOOD, Tapan; ROY, Somnath; PATHAK, Manabendra. Effect of pulse rate variation on blood flow through axisymmetric and asymmetric stenotic artery models. **Mathematical Biosciences**, v. 298, n. February, p. 1–18, 2018. <https://doi.org/10.1016/j.mbs.2018.01.008>

TIAN, Fang Bao; ZHU, Luoding; FOK, Pak Wing; LU, Xi Yun. Simulation of a pulsatile non-Newtonian flow past a stenosed 2D artery with atherosclerosis. **Computers in Biology and Medicine**, v. 43, n. 9, p. 1098–1113, 2013. <https://doi.org/10.1016/j.compbiomed.2013.05.023>

VIMMR, Jan; JONÁŠOVÁ, Alena. Non-Newtonian effects of blood flow in complete coronary and femoral bypasses. **Mathematics and Computers in Simulation**, v. 80, n. 6, p. 1324–1336, 2010. <https://doi.org/10.1016/j.matcom.2009.01.004>

VIMMR, Jan; JONÁŠOVÁ, Alena; BUBLÍK, Ondřej. Effects of three geometrical parameters on pulsatile blood flow in complete idealised coronary bypasses. **Computers and Fluids**, v. 69, p. 147–171, 2012. <https://doi.org/10.1016/j.compfluid.2012.08.007>

VIMMR, J.; JONÁŠOVÁ, A.; BUBLÍK, O. Numerical analysis of non-Newtonian blood flow and wall shear stress in realistic single, double and triple aorto-coronary bypasses. **International Journal for Numerical Methods in Biomedical Engineering**, v. 29, p. 1057–1081, 2013. <http://dx.doi.org/10.1002/cnm.2560>

WEDDELL, Jared C; KWACK, JaeHyuk; IMOUKHUEDE, P. I.; MASUD, Arif. Hemodynamic analysis in an idealized artery tree: Differences in wall shear stress between Newtonian and non-Newtonian blood models. **PLoS ONE**, v. 10, n. 4, p. 1–23, 2015. <http://dx.doi.org/10.1371/journal.pone.0124575>

ZINANI, Flávia; FREY, Sérgio. Galerkin least-squares multifield approximations for flows of inelastic non-Newtonian fluids. **Journal of Fluids Engineering**, v. 130, n. 8, p. 081507 1–14, 2008. <https://doi.org/10.1115/1.2956514>

ZYDNEY, A. L.; OLIVER, J. D.; COLTON, C. K. A constitutive equation for the viscosity of stored red cell suspensions: Effect of hematocrit, shear rate, and suspending phase. **Journal of Rheology**, v. 35, n. 8, p. 1639–1680, 1991. <http://dx.doi.org/10.1122/1.550249>